large instrumental noise ($\sim$70 $\mu$K per pixel)[4]. The difference between the observed cross-correlations implies that a small part (r.m.s. $\approx$ 1–2 $\mu$K) of the (COBE-WMAP) difference map is anti-correlated with the X-ray and radio maps. This is an unlikely occurrence (1 in 100) if the COBE instrument noise model is correct. There are known systematics in the COBE data[16] above this level, but the large instrument noise makes it difficult to ascertain whether this is the origin of the problem. In any case, the source of the discrepancy almost certainly lies with the COBE data, which contain much larger noise and systematic effects than the WMAP data. Thus, we believe the WMAP correlations presented here are robust. Further discussion of this and other issues are available as Supplementary Information.

The confidence levels that we quote (99.9% and 99.4%) are not primarily limited by experimental error, but by the fact that we can only observe a finite region of the Universe. We find it significant that both signals are consistent with the theoretical predictions with no free parameters. However, it should be emphasized that these two measurements are by no means independent. Both of them use the same CMB maps and, furthermore, the X-ray background is highly correlated with the NVSS radio sources[17]. If the distribution of sources of one of the maps by chance coincided with the fluctuations of the CMB, one would expect the other map also to be correlated with the CMB to some degree. The coincidence of the expected amplitudes of the two signals is encouraging but by no means definitive. On the other hand, the detection of the ISW-type signal in both CCFs gives a strong indication that they are not due to unknown systematic effects in the maps. The radio and X-ray data were gathered by quite distinct methods, and it would be surprising if unknown systematics in the two maps were correlated in any way. We will present more detailed analysis of these issues elsewhere.

We conclude that we have observed the ISW effect. If so, these observations offer the first direct glimpse into the production of CMB fluctuations, and provide important, independent confirmation of the new standard cosmological model: an accelerating universe, dominated by dark energy. It should be pointed out that measurements of the power spectrum of CMB fluctuations do not show evidence of increased power on large angular scales ($\theta > 20^\circ$) as predicted by the ISW effect, but rather indicate that there may be power missing[4]. Although this deficit is only at the $2\sigma$ level, it is intriguing, and may be telling us something about the formation of the very largest structures in the Universe. The consequences of the ISW effect reported here are primarily on intermediate angular scales, and are not in direct conflict with the power deficit on larger angular scales. Finally, we note that the WMAP-NVSS results have recently been independently analysed by the WMAP team, who find a similar level of correlation[18]. □

Received 15 April; accepted 8 October 2003; doi:10.1038/nature02139.


1. Bahcall, N., Ostriker, J. P., Perlmutter, S. & Steinhardt, P. The cosmic triangle: Revealing the state of the universe. *Science* **284,** 1481–1488 (1999).
2. Sachs, R. K. & Wolfe, A. M. Perturbations of a cosmological model and angular variations of the microwave background. *Astrophys. J.* **147,** 73–90 (1967).
3. Crittenden, R. & Turok, N. Looking for a cosmological constant with the Rees-Sciama effect. *Phys. Rev. Lett.* **76,** 575–578 (1996).
4. Bennett, C. L. *et al.* First year *Wilkinson Microwave Anisotropy Probe* observations: Preliminary maps and basic results. *Astrophys. J. Suppl.* **148,** 1–27 (2003).
5. Boldt, E. The cosmic X-ray background. *Phys. Rep.* **146,** 215–257 (1987).
6. Condon, J. *et al.* The NRAO VLA sky survey. *Astron. J.* **115,** 1693–1716 (1998).
7. Kinkhabwala, A. & Kamionkowski, M. New constraint on open cold-dark-matter models. *Phys. Rev. Lett.* **82,** 4172–4175 (1999).
8. Boughn, S. & Crittenden, R. Cross correlation of the CMB with radio sources: Constraints on an accelerating universe. *Phys. Rev. Lett.* **88,** 021302 (2002).
9. Boughn, S., Crittenden, R. & Koehrsen, G. The large scale structure of the X-ray background and its cosmological implications. *Astrophys. J.* **580,** 672–684 (2002).
10. Cowie, L. L., Barger, A. J., Bautz, M. W., Brandt, W. N. & Garmire, G. P. The redshift evolution of the 2–8 keV X-ray luminosity function. *Astrophys. J.* **584,** 57–60 (2003).
11. Dunlop, J. S. & Peacock, J. A. The redshift cut-off in the luminosity function of radio galaxies and quasars. *Mon. Not. R. Astron. Soc.* **247,** 19–42 (1990).
12. Boughn, S., Crittenden, R. & Turok, N. Correlations between the cosmic X-ray and microwave backgrounds: Constraints on a cosmological constant. *New Astron.* **3,** 275–291 (1998).
13. Bennett, C. L. *et al.* First year *Wilkinson Microwave Anisotropy Probe* observations: Foreground emission. *Astrophys. J. Suppl.* **148,** 97–117 (2003).
14. Tegmark, M., de Oliveira-Costa, A. & Hamilton, A. A high resolution foreground cleaned CMB map from WMAP. Preprint at ⟨http://xxx.lanl.gov/astro-ph/0302496⟩ (2003).
15. Peiris, H. V. & Spergel, D. N. Cross-correlating the Sloan Digital Sky Survey with the microwave sky. *Astrophys. J.* **540,** 605–613 (2000).
16. Kogut, A. *et al.* Calibration and systematic error analysis for the COBE DMR 4 year sky maps. *Astrophys. J.* **470,** 653–673 (1996).
17. Boughn, S. Cross-correlation of the 2–10 keV X-ray background with radio sources: Constraining the large-scale structure of the X-ray background. *Astrophys. J.* **499,** 533–541 (1998).
18. Nolta, M.R. *et al.* First year *Wilkinson Microwave Anisotropy Probe* observations: Dark energy induced correlation with radio sources. Preprint at ⟨http://xxx.lanl.gov/astro-ph/0305907⟩ (2003).
19. Spergel, D. N. *et al.* First year *Wilkinson Microwave Anisotropy Probe* observations: Determination of cosmological parameters. *Astrophys. J. Suppl.* **148,** 175–194 (2003).


**Supplementary Information** accompanies the paper on **www.nature.com/nature**.

**Acknowledgements** We are grateful to M. Nolta, L. Page and the rest of the WMAP team, as well as to N. Turok, B. Partridge and B. Bassett, for useful conversations. R.C. acknowledges financial support from a PPARC fellowship.

**Competing interests statement** The authors declare that they have no competing financial interests.

**Correspondence** and requests for materials should be addressed to R.C. (Robert.Crittenden@port.ac.uk).

# A large population of 'Lyman-break' galaxies in a protocluster at redshift $z \approx 4.1$

**George K. Miley[1], Roderik A. Overzier[1], Zlatan I. Tsvetanov[2], Rychard J. Bouwens[3], Narciso Benítez[2], John P. Blakeslee[2], Holland C. Ford[2], Garth D. Illingworth[3], Marc Postman[4], Piero Rosati[5], Mark Clampin[4], George F. Hartig[4], Andrew W. Zirm[1], Huub J. A. Röttgering[1], Bram P. Venemans[1], David R. Ardila[2], Frank Bartko[6], Tom J. Broadhurst[7], Robert A. Brown[2], Chris J. Burrows[2], E. S. Cheng[8], Nicholas J. G. Cross[2], Carlos De Breuck[5], Paul D. Feldman[2], Marijn Franx[1], David A. Golimowski[2], Caryl Gronwall[2], Leopoldo Infante[9], André R. Martel[2], Felipe Menanteau[2], Gerhardt R. Meurer[2], Marco Sirianni[2], Randy A. Kimble[8], John E. Krist[6], William B. Sparks[4], Hien D. Tran[2], Richard L. White[4] & Wei Zheng[2]**

[1]*Leiden Observatory, University of Leiden, PO Box 9513, Leiden, 2300 RA, The Netherlands*
[2]*Department of Physics & Astronomy, Johns Hopkins University, Baltimore, Maryland 21218, USA*
[3]*Lick Observatory, University of California, Santa Cruz, California 95064, USA*
[4]*Space Telescope Science Institute, Baltimore, Maryland 21218, USA*
[5]*European Southern Observatory, Garching, D-85748, Germany*
[6]*Bartko Science & Technology, Mead, Colorado 80542-0670, USA*
[7]*The Racah Institute of Physics, Hebrew University, Jerusalem, 91904, Israel*
[8]*NASA-Goddard Space Flight Centre, Greenbelt, Maryland 20771, USA*
[9]*Departmento de Astronomía y Astrofísica, Pontificia Universidad Católica de Chile, Casilla 306, Santiago 22, Chile*

**The most massive galaxies and the richest clusters are believed to have emerged from regions with the largest enhancements of mass density[1–4] relative to the surrounding space. Distant radio galaxies may pinpoint the locations of the ancestors of rich clusters, because they are massive systems associated with 'over-densities' of galaxies that are bright in the Lyman-α line of hydrogen[5–7]. A powerful technique for detecting high-redshift galaxies is to search for the characteristic 'Lyman break' feature in the galaxy colour, at wavelengths just shortwards of Lyα, which is due to absorption of radiation from the galaxy by the**

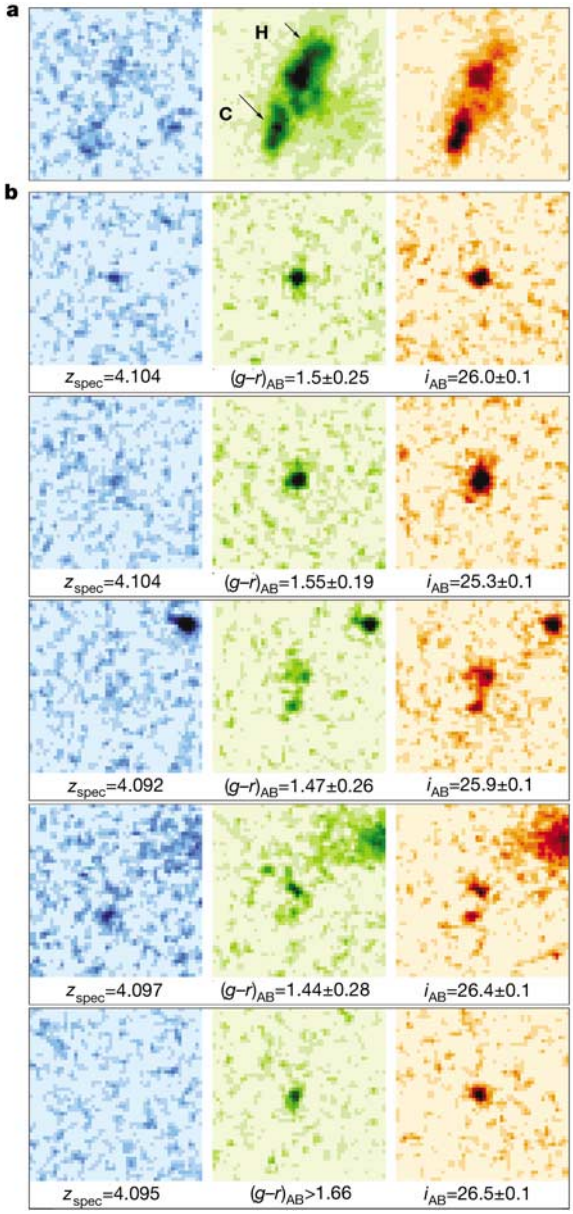


**Figure 1** Deep images of Lyα-emitting protocluster galaxies. Images show galaxy morphologies observed through three filters: g band (left), r band (middle) and i band (right). Each 2.5″ × 2.5″ image has been smoothed by a gaussian function with a full-width at half-maximum of 1.5 pixels (0.074″). The observations were carried out between 8 and 12 July 2002 with the Wide Field Channel of the ACS[21]. The total observing time of 13 orbits was split over the broad-band filters F475W (g band, four orbits), F625W (r band, four orbits) and F775W (i band, five orbits), thereby bracketing redshifted Lyα at 6,214 Å. During each orbit, two 1,200-s exposures were made, to facilitate the removal of cosmic rays. The observations were processed through the ACS GTO pipeline[26] to produce registered, cosmic-ray-rejected images. The limiting $2\sigma$ magnitudes in a 0.2-arcsec$^2$ aperture were 28.71 (F475W), 28.44 (F625W) and 28.26 (F775W). Object detection and photometry were then obtained using SExtractor[27]. **a**, The clumpy radio galaxy TN J1338–1942 at $z = 4.1$. This is the brightest galaxy in the protocluster and inferred to be the dominant cluster galaxy in the process of formation. Because the equivalent width of Lyα is large (~500 Å), the r band is dominated by Lyα. Arrows indicate the positions[8] of the radio core (C) and the northern hotspot (H). The Lyα emission is elongated in the direction of the radio emission and the large-scale Lyα halo[7] with a projected linear size of ~15 kpc (assuming $H_0 = 65\,\mathrm{km\,s^{-1}Mpc^{-1}}$, $\Omega_M = 0.3$, $\Omega_\Lambda = 0.7$). **b**, Images of five spectroscopically confirmed Lyα emitters in the protocluster. Listed below each galaxy are its spectroscopic redshift[7], the magnitude of the observed Lyman break, and the i-band magnitude. Two of the Lyα emitters are clumpy, as expected from young galaxies.

**intervening intergalactic medium. Here we report multicolour imaging of the most distant candidate[7–9] protocluster, TN J1338–1942 at a redshift $z \approx 4.1$. We find a large number of objects with the characteristic colours of galaxies at that redshift, and we show that this excess is concentrated around the targeted dominant radio galaxy. Our data therefore indicate that TN J1338–1942 is indeed the most distant cluster progenitor of a rich local cluster, and that galaxy clusters began forming when the Universe was only ten per cent of its present age.**

There is increasing evidence that structures of galaxies existed in the early Universe, but the detection of protoclusters at redshifts $z > 1$ using conventional optical and X-ray techniques is difficult[10–12]. Some of us have developed an efficient method for pinpointing distant protoclusters. The technique is based on the hypothesis that the most powerful known high-redshift radio galaxies are frequently associated with massive forming galaxies[13–16] in protoclusters[5]. As a first step towards testing this hypothesis, we recently conducted a large programme with the Very Large Telescope (VLT) of the European Southern Observatory to search for galaxy overdensities associated with protoclusters around luminous high-redshift radio galaxies. Deep narrow- and broad-band imaging was used to locate candidate galaxies having bright Lyα emission, and follow-up spectra have confirmed that most of these candidates have similar redshifts to the high-redshift radio galaxies. All five targets studied with the VLT to sufficient depth have >20 spectroscopically confirmed Lyα and/or Hα companion galaxies, associated with

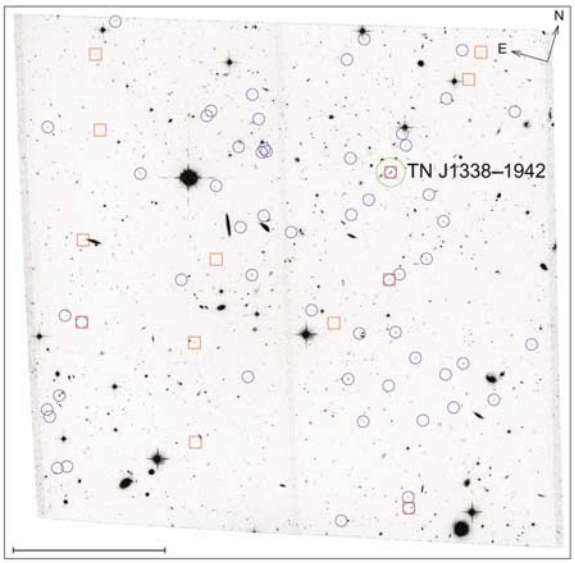


**Figure 2** The spatial distribution of g-band dropout objects. Superimposed on the combined 3.4′ × 3.4′ ACS greyscale image are the locations of g-band dropout objects (blue circles), selected to have colours and magnitudes of $(g–r) \geq 1.5$, $(g–r) \geq (r–i) + 1.1$, $(r–i) \leq 1$ and $i < 27$. In addition, objects were required to have a SExtractor[27] stellarity parameter of less than 0.85 to ensure that the sample was not contaminated by stars. These criteria filter galaxies having Lyman breaks at $z \approx 4$, thereby providing a sample of protocluster Lyman-break galaxy candidates. We detected 30 g-dropout objects in the field around TN J1338–1942 with $i_{775} < 26$, and 56 with $i_{775} < 27$.The number of g-band dropout objects is anomalously large, and their distribution is concentrated within a circular region of ~1′ in radius that includes the radio galaxy TN J1338–1942 (large green circle). Also shown are the positions of the spectroscopically confirmed Lyα emitters (red squares). Because the selection criteria were optimized to detect Lyman-break galaxies, some of the Lyα emitters did not fall into the formal sample of Lyman-break galaxies. The measured excess and its spatial clustering are evidence that a substantial fraction of the g-band dropout objects are Lyman-break galaxies associated with the protocluster. (See Fig. 1 legend for further details about the observations and the subsequent analysis.) Scale bar, 1′.

galaxy overdensities[6,7]. Their formal velocity dispersions are a few hundred km s$^{-1}$, but there was not enough time since the Big Bang for them to have become virialized. The scale sizes of the structures inferred from their spatial boundaries are ~3–5 Mpc. Assuming that the overdensities are due to a single structure, the masses derived from the observed structure sizes and overdensities are comparable to those of clusters of galaxies in the local Universe[7]. These observations led us to hypothesize that the overdensities of Lyα galaxies around radio sources are due to the fact that they are in protoclusters.

Galaxies that emit strong Lyα comprise only a small fraction of distant galaxies, and are biased towards non-dusty objects and galaxies that are undergoing the most vigorous star formation. Only about 25% of $z \approx 3$ galaxies have Lyα equivalent widths detectable by our VLT narrow-band imaging searches[17,18]. If the overdensities of Lyα galaxies are located in protoclusters, additional galaxy populations should be present and detectable on the basis of characteristic continuum features in the galaxy spectra. The most important of these features is the sharp 'Lyman break' blueward of Lyα, caused by the absorption of the galaxy continuum radiation by neutral hydrogen clouds along the line of sight. Searching for Lyman-break galaxies is a powerful technique for finding high-redshift galaxies[11,19,20].

Because of its high spatial resolution, large field of view and excellent sensitivity, the Advanced Camera for Surveys[21] (ACS) on the Hubble Space Telescope is uniquely suited for studying the morphologies of galaxies in the protoclusters and for finding additional galaxies on the basis of the Lyman-break features in their spectra. We therefore used the ACS to observe the most distant of our VLT protoclusters, TN J1338–1942 (ref. 7) at $z = 4.1$. This is a structure with 21 spectroscopically confirmed Lyα emitters and a rest-frame velocity dispersion of 325 km s$^{-1}$. Images were taken through three 'Sloan' filters—g band centred at 4,750 Å, r band centred near 6,250 Å and i band centred near 7,750 Å. These filters were chosen so that their wavelength responses bracketed redshifted Lyα at 6,214 Å and were sensitive to the Lyman-break feature blueward of Lyα.

A $3.4' \times 3.4'$ field was observed, with the radio galaxy located $\sim 1'$ from the image centre. Besides the radio galaxy, this field covered 12 of the 21 known Lyα emitting galaxies in the candidate protocluster. All 12 objects were detected in both r band and i band, with i-band magnitudes ranging from 25 to 28, compared with $23.3 \pm 0.03$ for the radio galaxy. As illustrated in Fig. 1, these objects were either absent or substantially attenuated in the g band, and their *g*–*r* colours are generally consistent with predicted values of Lyman breaks[22]. Half of the objects are extended in $i_{775}$, and three of these are resolved into two distinct knots of continuum emission, suggestive of merging.

We next used the Lyman-break technique to search for a population of Lyman-break galaxies in the protocluster that do not emit strong Lyα and would therefore have been undetectable in our VLT observations. Evidence for the existence of such a population was sought by analysing the number and spatial distribution of 'g-band dropout' objects—that is, objects whose colours are consistent with Lyman breaks in their spectra at the redshift of the protocluster. To investigate whether there is a statistically significant excess of such g-band dropout objects, we estimated the surface density and cosmic variance of g-band dropouts in a typical ACS field observed with the same filters and to the same depth as TN J1338–1942. We did this by cloning[23] $B_{435}$-band dropouts in 15 different pointings from the southern field of the Great Observatories Origins Deep Survey (GOODS)[24]. Results indicate that the number of g-band dropouts in our field is a factor of 2.5 times higher than the average number found in a random GOODS field. Taking account of the typical cosmic variance[25] in the distribution of $z \approx 4$ Lyman-break galaxies, this is a $3\sigma$ excess on the assumption that the distribution function is gaussian. Further evidence that a substantial fraction of these g-dropout objects are Lyman-break galaxies associated with the protocluster is provided by the strong concentration of the g-band dropouts in a cluster-sized region around the radio galaxy. This is illustrated in Fig. 2. More than half of the g-band dropouts are located in a region of $\sim 1'$ in radius (corresponding to a diameter of ~1 Mpc at $z = 4.1$). The number of g-band dropouts in this region is a factor of 5 times the average number encountered in similarly sized regions that are randomly drawn from the GOODS survey. This is a $5\sigma$ excess, indicating that the number of g-band dropouts in our field is anomalously high at greater than the 99% confidence level. The spatial non-uniformity of g-band dropout objects in our field becomes even more pronounced when fainter objects down to a magnitude of $i = 27$ are included (Fig. 2).

Are there alternative explanations for the observed excess of g-band dropout objects other than a population of Lyman-break galaxies at $z \approx 4.1$? An object with a Balmer break at $z \approx 0.5$ could also be observed as a g-band dropout object. However, a population of such $z \approx 0.5$ objects would also be present in the GOODS comparison sample. Although the existence of an intervening structure of Balmer-break galaxies at $z \approx 0.5$ cannot be completely ruled out, its coincidence in location with the $z \approx 4.1$ structure of Lyα galaxies and the faintness and small sizes of the observed objects make this possibility highly unlikely.

The spatial coincidence of the excess in g-band dropout objects with the previously detected overdensity of Lyα emitters around a forming massive galaxy is strong evidence that we are observing a new population of Lyman-break galaxies in a protocluster. This would mean that TN J1338–1942, at $z \approx 4.1$, is indeed the most distant known protocluster, and that distant luminous radio galaxies pinpoint the progenitors of nearby rich clusters. Such protoclusters provide an opportunity to study the development of galaxies and clusters in the early Universe. They provide samples of different galaxy populations at the same distance, whose morphologies and spectral energy distributions could be used to disentangle the evolution and star formation history of different types of galaxies. The topological information that could be derived by mapping the shapes and sizes of such protoclusters over larger areas could answer the question of whether the first protoclusters in the early Universe formed in sheets or filaments. □

Received 15 July; accepted 9 October 2003; doi:10.1038/nature02125.


1. Kaiser, N. On the spatial correlation function of Abell clusters. *Astrophys. J.* **284,** L9–L12 (1984).
2. White, S. D. M. & Rees, M. J. Core condensation in heavy halos—A two-stage theory for galaxy formation and clustering. *Mon. Not. R. Astron. Soc.* **183,** 341–358 (1978).
3. Baugh, C. M., Cole, S., Frenk, C. S. & Lacey, C. G. The epoch of galaxy formation. *Astrophys. J.* **498,** 504–521 (1998).
4. Bahcall, N. A. & Fan, X. The most massive distant clusters: Determining Ω and $\sigma_8$. *Astrophys. J.* **504,** 1–6 (1998).
5. Miley, G. in *Extrasolar Planets to Cosmology: The VLT Opening Symposium* (eds Bergeron, J. & Renzini, A.) 32–42 (Springer, Berlin, 2000).
6. Pentericci, L. *et al.* A search for clusters at high redshift. II. A proto cluster around a radio galaxy at z = 2.16. *Astron. Astrophys.* **361,** L25–L28 (2000).
7. Venemans, B. P. *et al.* The most distant structure of galaxies known: A protocluster at z = 4.1. *Astrophys. J.* **569,** L11–L14 (2002).
8. De Breuck, C. *et al.* VLT spectroscopy of the z = 4.11 radio galaxy TN J1338–1942. *Astron. Astrophys.* **352,** L51–L56 (1999).
9. De Breuck, C., van Breugel, W., Röttgering, H. J. A. & Miley, G. A sample of 669 ultra steep spectrum radio sources to find high redshift radio galaxies. *Astron. Astrophys. Suppl.* **143,** 303–333 (2000).
10. Rosati, P. *et al.* An X-ray-selected galaxy cluster at z = 1.26. *Astron. J.* **118,** 76–85 (1999).
11. Steidel, C. C. *et al.* A large structure of galaxies at redshift z ~ 3 and its cosmological implications. *Astrophys. J.* **492,** 428–438 (1998).
12. Shimasaku, K. *et al.* Subaru deep survey IV: Discovery of a large-scale structure at redshift ~ = 5. *Astrophys. J.* **586,** L111–L114 (2003).
13. De Breuck, C. *et al.* Optical and near-infrared imaging of ultra-steep-spectrum radio sources: The K-z diagram of radio-selected and optically selected galaxies. *Astron. J.* **123,** 637–677 (2002).
14. Dey, A., van Breugel, W., Vacca, W. D. & Antonucci, R. Triggered star formation in a massive galaxy at z = 3.8: 4C 41.17. *Astrophys. J.* **490,** 698–709 (1997).
15. Pentericci, L. *et al.* HST images and properties of the most distant radio galaxies. *Astrophys. J.* **504,** 139–146 (1999).
16. van Ojik, R. *Gas in Distant Radio Galaxies: Probing the Early Universe* Thesis, Leiden Univ. (1995).
17. Steidel, C. C. *et al.* Lyα imaging of a proto-cluster region at ⟨z⟩ = 3.09. *Astrophys. J.* **532,** 170–182 (2000).
18. Shapley, A. E., Steidel, C. C., Pettini, M. & Adelberger, K. Rest-frame ultraviolet spectra of z ~ 3 Lyman break galaxies. *Astrophys. J.* **588,** 65–89 (2003).

19. Steidel, C. C., Giavalisco, M., Pettini, M., Dickinson, M. & Adelberger, K. Spectroscopic confirmation of a population of normal star-forming galaxies at redshifts z > 3. *Astrophys. J.* **462,** L1–L7 (1999).
20. Steidel, C. C., Adelberger, K., Giavalisco, M., Dickinson, M. & Pettini, M. Lyman-break galaxies at z > 4 and the evolution of the ultraviolet luminosity density at high redshift. *Astrophys. J.* **519,** 1–17 (1999).
21. Ford, H. C. *et al.* Advanced camera for the Hubble Space Telescope. *Proc. SPIE* **3356,** 234–248 (1998).
22. Madau, P. Radiative transfer in a clumpy universe: The colors of high-redshift galaxies. *Astrophys. J.* **441,** 18–27 (1995).
23. Bouwens, R. J., Broadhurst, T. & Illingworth, G. Cloning dropouts: Implications for galaxy evolution at high redshift. *Astrophys. J.* **593,** 640–660 (2003).
24. Giavalisco, M. *et al.* The Great Observatories Origins Deep Survey. *Astrophys. J. Lett.* (special issue) (in the press).
25. Somerville, R. S. *et al.* Cosmic variance in the Great Observatories Origins Deep Survey. *Astrophys. J. Lett.* (special issue) (in the press); preprint at ⟨http://xxx.lanl.gov/astro-ph/0309071⟩ (2003).
26. Blakeslee, J. P., Anderson, K. R., Meurer, G. R., Benítez, N. & Magee, D. An automatic image reduction pipeline for the Advanced Camera for Surveys. *ASP Conf. Ser.* **295,** 257–260 (2003).
27. Bertin, E. & Arnouts, S. SExtractor: Software for source extraction. *Astron. Astrophys.* **117,** 393–404 (1996).

**Competing interests statement** The authors declare that they have no competing financial interests.

**Correspondence** and requests for materials should be addressed to G.K.M. (miley@strw.leidenuniv.nl).

# Coherent spin manipulation without magnetic fields in strained semiconductors

**Y. Kato, R. C. Myers, A. C. Gossard & D. D. Awschalom**

*Center for Spintronics and Quantum Computation, University of California, Santa Barbara, California 93106, USA*

**A consequence of relativity is that in the presence of an electric field, the spin and momentum states of an electron can be coupled; this is known as spin–orbit coupling. Such an interaction opens a pathway to the manipulation of electron spins within non-magnetic semiconductors, in the absence of applied magnetic fields. This interaction has implications for spin-based quantum information processing[1] and spintronics[2,3], forming the basis of various device proposals[4–8]. For example, the concept of spin field-effect transistors[4,5] is based on spin precession due to the spin–orbit coupling. Most studies, however, focus on non-spin-selective electrical measurements in quantum structures. Here we report the direct measurement of coherent electron spin precession in zero magnetic field as the electrons drift in response to an applied electric field. We use ultrafast optical techniques to spatiotemporally resolve spin dynamics in strained gallium arsenide and indium gallium arsenide epitaxial layers. Unexpectedly, we observe spin splitting in these simple structures arising from strain in the semiconductor films. The observed effect provides a flexible approach for enabling electrical control over electron spins using strain engineering. Moreover, we exploit this strain-induced field to electrically drive spin resonance with Rabi frequencies of up to ~30 MHz.**

Even in the absence of a magnetic field, the conduction band of a semiconductor lacking an inversion centre has spin splitting away from the zone centre, owing to spin–orbit coupling. For example, the zinc blende crystal structure of GaAs has bulk inversion asymmetry (BIA), while heterostructures can introduce structural inversion asymmetry (SIA). BIA gives rise to the Dresselhaus spin splitting[9], which has a quantization axis perpendicular to the electron wavevector **k**, and changes its orientation with respect to **k** as the direction of **k** changes between the crystal directions [110] and [1$\bar{1}$0]. Meanwhile, SIA gives rise to the Rashba hamiltonian[10] ($H_R = \alpha(\mathbf{k} \times \hat{\mathbf{n}})\cdot\boldsymbol{\sigma}$, where $\alpha$ is the Rashba coefficient and $\boldsymbol{\sigma}$ is the Pauli operator) and introduces an effective magnetic field perpendicular to **k** and the symmetry-breaking axis $\hat{\mathbf{n}}$, but its relative orientation to **k** remains constant in the plane normal to $\hat{\mathbf{n}}$. For example, two-dimensional electron gases in semiconductor heterostructures have zero-magnetic-field splitting as a consequence of these mechanisms[11,12], and have been studied through the beatings in the Shubnikov de Haas oscillations[13,14], analysis of the antilocalization peak in magnetoresistance measurements[15,16], and spin-flip Raman scattering[17]. Gate-voltage control of the Rashba interaction has also been demonstrated in these structures[18]. Additionally, it has been predicted that these interactions may cause spin precession in the diffusive transport regime[19]. Although electrons scatter between many states with different **k**, the application of an electric field should result in a non-zero average of the effective magnetic field that can coherently rotate the spins.

Here we report a similar spin splitting in bulk semiconductors originating from strain. We observe coherent electron spin precession angles exceeding 3$\pi$ in zero magnetic field as the spins drift distances of greater than 60 $\mu$m in ~13 ns. Samples grown by molecular beam epitaxy[20] consist of a 2-$\mu$m n-GaAs layer ($n = 3 \times 10^{16}$ cm$^{-3}$) acting as a spin probe layer at the surface, and a 2-$\mu$m film of $Al_{0.4}Ga_{0.6}As$ underneath serving as a stressor/etch-stop layer. The semi-insulating GaAs (001) substrate is removed by chemical etching in order to form a rectangular membrane ~100 $\mu$m by ~300 $\mu$m. The processed membrane has curvature, possibly owing to the larger lattice constant or the oxidation of the $Al_{0.4}Ga_{0.6}As$ layer, thereby straining the n-GaAs film. Ni/GeAu ohmic contacts are formed on the surface in order to apply an in-plane electric field $E$ along [1$\bar{1}$0].

Time- and spatially resolved Faraday rotation (FR) spectroscopy[21,22] is used to probe the electron spin dynamics. In this pump–probe measurement, the FR of the probe beam measures the total magnetization of the optically injected electron spins in the growth direction $z$. The laser beams are normally incident on the sample and focused to spots with full-width at half-maximum of 14 $\mu$m, whose relative distance $d$ along the direction of $E$ can be controlled with a stepper-motor-driven mirror, enabling spatial scanning in one dimension. All the measurements are taken at temperature $T = 5$ K in a magneto-optical cryostat, and the external

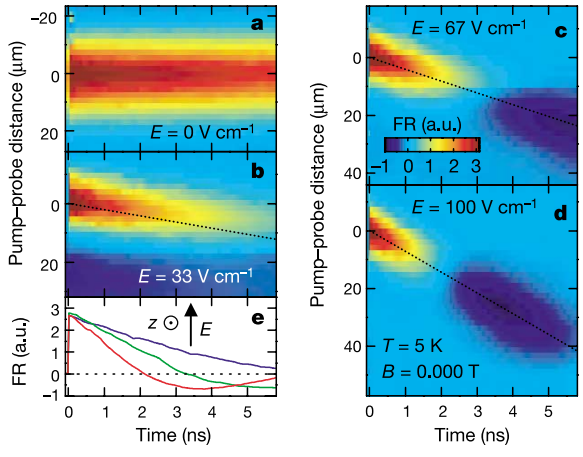


**Figure 1** Spatiotemporal evolution of a spin packet at zero magnetic field. **a**–**d**, FR as a function of temporal and spatial separation between pump and probe pulses for $E = 0$, 33, 67, 100 V cm$^{-1}$, respectively. Data in **a** have been multiplied by 0.67 for clarity, and all panels share the colour scale shown in **c**. The dotted lines have slopes determined by the spin drift velocity. The slight negative signal in the left bottom corner of **b** is due to an older spin packet created by a previous pulse. **e**, Line sections along dotted lines in **b** (blue), **c** (green) and **d** (red). Inset shows the geometry. Zero external magnetic field was calibrated by the resonant spin amplification peak at $E = 0$ V cm$^{-1}$.